Stem Cells Translational Medicine, 2024, **13**, 293–308
https://doi.org/10.1093/stcltm/szad090
Advance access publication 30 December 2023
Original Research

Histone Trimethylations and HDAC5 Regulate Spheroid Subpopulation and Differentiation Signaling of Human Adipose-Derived Stem Cells

Ming-Min Chang[1,2], Yi-Kai Hong[3,4], Chao-Kai Hsu[3,4], Hans I-Chen Harn[5], Bu-Miin Huang[1], Ya-Hsin Liu[6], Fu-I Lu[7], Yuan-Yu Hsueh[4,8,9], Shau-Ping Lin[10], Chia-Ching Wu[*,1,4,11,12]

[1]Department of Cell Biology and Anatomy, College of Medicine, National Cheng Kung University, Tainan, Taiwan
[2]Medical Device Innovation Center, National Cheng Kung University, Tainan, Taiwan
[3]Department of Dermatology, College of Medicine, National Cheng Kung University, Tainan, Taiwan
[4]International Center for Wound Repair and Regeneration, National Cheng Kung University, Tainan, Taiwan
[5]Department of Pathology, Keck School of Medicine, University of Southern California, Los Angeles, CA, USA
[6]Department of Life Sciences, College of Bioscience and Biotechnology, National Cheng Kung University, Tainan, Taiwan
[7]Department of Biotechnology and Bioindustry Sciences, College of Bioscience and Biotechnology, National Cheng Kung University, Tainan, Taiwan
[8]Division of Plastic and Reconstructive Surgery, Department of Surgery, National Cheng Kung University Hospital, College of Medicine, National Cheng Kung University, Tainan, Taiwan
[9]Institute of Clinical Medicine, College of Medicine, National Cheng Kung University, Tainan, Taiwan
[10]Institute of Biotechnology, College of Bio-Resources and Agriculture, National Taiwan University, Taipei, Taiwan
[11]Institute of Basic Medical Sciences, College of Medicine, National Cheng Kung University, Tainan, Taiwan
[12]Department of Biomedical Engineering, National Cheng Kung University, Tainan, Taiwan

[*]Corresponding author: Chia-Ching Wu, PhD, Department of Cell Biology and Anatomy, College of Medicine, National Cheng Kung University, University, No. 1 University Road, Tainan 70101, Taiwan. Tel: +886 6 2353535 ext. 5327; Fax: +886 6 209 3007; Email: joshccwu@mail.ncku.edu.tw

Abstract

Human adipose-derived stem cells (ASCs) have shown immense potential for regenerative medicine. Our previous work demonstrated that chitosan nano-deposited surfaces induce spheroid formation and differentiation of ASCs for treating sciatic nerve injuries. However, the underlying cell fate and differentiation mechanisms of ASC-derived spheroids remain unknown. Here, we investigate the epigenetic regulation and signaling coordination of these therapeutic spheroids. During spheroid formation, we observed significant increases in histone 3 trimethylation at lysine 4 (H3K4me3), lysine 9 (H3K9me3), and lysine 27 (H3K27me3), accompanied by increased histone deacetylase (HDAC) activities and decreased histone acetyltransferase activities. Additionally, HDAC5 translocated from the cytoplasm to the nucleus, along with increased nuclear HDAC5 activities. Utilizing single-cell RNA sequencing (scRNA-seq), we analyzed the chitosan-induced ASC spheroids and discovered distinct cluster subpopulations, cell fate trajectories, differentiation traits, and signaling networks using the 10x Genomics platform, R studio/language, and the Ingenuity Pathway Analysis (IPA) tool. Specific subpopulations were identified within the spheroids that corresponded to a transient reprogramming state (Cluster 6) and the endpoint cell state (Cluster 3). H3K4me3 and H3K9me3 were discovered as key epigenetic regulators by IPA to initiate stem cell differentiation in Cluster 6 cells, and confirmed by qPCR and their respective histone methyltransferase inhibitors: SNDX-5613 (a KMT2A inhibitor for H3K4me3) and SUVi (an SUV39H1 inhibitor for H3K9me3). Moreover, H3K9me3 and HDAC5 were involved in regulating downstream signaling and neuronal markers during differentiation in Cluster 3 cells. These findings emphasize the critical role of epigenetic regulation, particularly H3K4me3, H3K9me3, and HDAC5, in shaping stem cell fate and directing lineage-specific differentiation.

Key words: sphere formation; adipose-derived stem cells; histone trimethylation; HDAC5; single-cell RNA sequencing; differentiation potential.

Received: 1 August 2023; Accepted: 16 November 2023.

Graphical Abstract

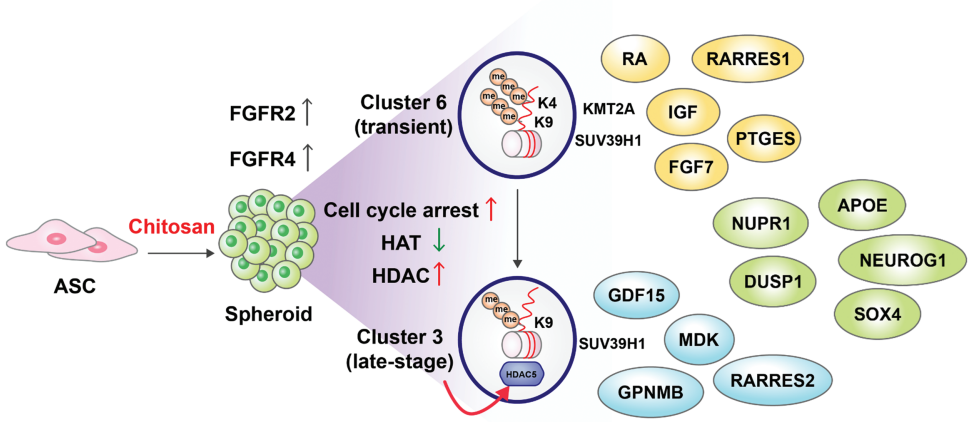

Significance Statement

This study unravels the pivotal role of histone trimethylations and HDAC5 in regulating spheroid subpopulations and differentiation signaling of human adipose-derived stem cells on the chitosan surface. In transient state (Cluster 6) cells, KMT2A (H3K4me3) and SUV39H1 (H3K9me3) increase RARRES1, IGF, FGF7, and PTGES to initiate stem cell reprogramming. In endpoint state (Cluster 3) cells, H3K9me3 and HDAC5 upregulate RARRES2, GDF15, MDK, and GPNMB to guide stem cell fate decisions. Other differentiation-related genes such as APOE, DUSP1, NUPR1, NEUROG1, and SOX4 are also upregulated in both Clusters 3 and 6, leading to neuronal lineage cells. By understanding the epigenetic mechanisms involved in shaping stem cell fate and guiding lineage-specific differentiation, our findings may contribute to advancing regenerative medicine and therapeutic strategies for treating sciatic nerve injuries and other neurological disorders.

Introduction

Adipose-derived stem cells (ASCs), a subset of bone marrow mesenchymal stem cells (BMMSCs), can be relatively easily harvested from subcutaneous adipose tissue through liposuction surgery, offering a high yield with minimal donor-site morbidity.[1,2] The use of human ASCs in regenerative medicine is highly attractive due to ethical advantages over embryonic stem cells (ESCs). Additionally, numerous studies have explored the safety and efficacy of implanting ASCs in different animal models.[3,4] With similar differentiation ability to BMMSCs, the transplantation of ASCs has been reported to promote repair and regeneration in neural,[5–7] bone,[8,9] vocal fold,[10] and cardiovascular tissues.[11] ASCs have also exhibited the potential to differentiate toward mesodermal (adipocytes, osteoblasts, and chondrocytes), ectodermal (neurons and glial cells), and endodermal (hepatocytes and pancreatic β-cells) lineage upon in vitro induction.[1,12–14] High-density culturing of ASCs in neurobasal medium (NBM) supplemented with B27 induces the formation of compact free-floating neurospheroids,[15] which can be further differentiated into neuronal, glial, and oligodendrocyte cells by adding epidermal growth factor (EGF), basic fibroblast growth factor (bFGF), and brain-derived neurotrophic factor (BDNF).[16–18] The differentiation of BMMSCs into neurospheres can also be achieved by seeding cells on ultra-low-attachment surfaces in NBM supplemented with B27, EGF, bFGF,[19] and further differentiated into Schwann-cell-like cells, oligodendrocyte precursors, or sensory neuron.[20–22] Morphological changes and the induction of spheroid formation can also be triggered by seeding the ASCs on chitosan nano-deposited surface, resulting in a mixed population of neural linage cells expressing nestin, neural filament heavy chain (NFH), and glial fibrillary acidic protein (GFAP).[17,23–25] The addition of FGF9 during spheroids formation further promotes fate commitment toward Schwann cell linage via FGF9-FGFR2-Akt signaling pathway.[17]

Differentiation, reprogramming, and direct reprogramming of stem cells are accompanied by drastic changes in both gene and epigenetic regulations. Epigenetic factors, including histone modifications, DNA methylation, and non-coding RNA-mediated regulations, are known to play a pivotal role in controlling stem cell fate for differentiation, reprogramming, and direct reprogramming.[26] Chromatin regulation is a fundamental mechanism underlying stem cell pluripotency, differentiation, and the establishment of cell type-specific gene expression profiles. Histone methylation and acetylation are two major modifications acting as gene transcriptional regulators for various cellular functions and responses. Histone methylation can activate or repress gene transcription, depending on which residue is methylated. Most histone modifications involve sites within the first 30 amino acids of the N-terminal domains of histones, such as histone 3 at lysine 4 (H3K4), lysine 9 (H3K9), and lysine 27 (H3K27).[27] Methylation of H3K4 is the most common modification to active transcription genes, whereas the methylation of H3K9 and H3K27 is usually associated with gene silence.[26] A chromatin landscape analysis reported that human ESCs have abundant acetylation marks at H3K9, H3K56, H4K5, H4J48, H4K12, and H4K16, whereas in differentiated cells have high levels of the repressive marks at H3K9me2/me3, H3K27me1/me2, H3K35me2, and H4K20me2.[28] The H3K27me3 is critical to the "stemness" of stem cells, as H3K27me2 triggers cellular differentiation.[29] Additionally, H3K4 and H3K27 are

associated together as a "bivalent" chromatin signature to mark genes that are repressed in hESCs but poised to allow for alternative fate.[29–31] Dynamic changes in histones H3K4, H3K9, and H3K27 trimethylation on nestin locus after the stimulation of EGF, bFGF, and B27 have been reported.[32] However, the detailed mechanism underlying the histone trimethylation-mediated differentiation of ASCs during spheroid formation is not yet fully understood.

Histone acetylation is dynamic and reversible through two antagonistic enzymes: histone acetyltransferases (HATs) and histone deacetylases (HDACs), which open chromatin structure or inactive the transcription, respectively.[33] HATs can maintain the stemness property of many stem cells, including ESCs,[33,34] MSCs,[35] neural stem cells (NSCs),[36] and hematopoietic stem cells.[37] Dysregulation of HAT-mediated histone acetylation leads to a reduced potential of self-renewal in stem cells.[38] There are 18 HDACs in mammalian genomes, classified into 4 classes: Class I (HDAC1, HDAC2, HDAC3, and HDAC8), Class IIa (HDAC4, HDAC5, HDAC7, and HDAC9), IIb (HDAC6 and HDAC10), Class III (SIRT 1-7), and Class IV (HDAC11). In Class I HDACs, HDAC1 and HDAC2 are expressed in the nuclear and formed multiprotein enzyme complexes for cell division and stem cell self-renewal by maintaining pluripotent transcriptional factors.[39] HDAC1 and HDAC2 are also essential for differentiating neuronal precursors into neurons.[40] Class II HDACs can shuttle between the nucleus and cytoplasm, depending on their phosphorylation status, and have tissue-specific expression patterns. Class IIa HDACs contain a myocyte enhancer factor-2 (MEF2) binding site to repress MEF2-mediated transcription, thereby controlling the differentiation of cardiac, neural, and dental pulp stem cells.[41] HDAC5 is implicated in neuronal differentiation by decreasing acetylated tubulin to promote axon regeneration in injured dorsal root ganglia (DRG) neurons.[42] HDAC6 and HDAC10 of Class IIb HDACs are primarily located in the cytoplasm. Until now, the histone modification mechanisms underlying ASCs, especially during morphological change or differentiation, are largely unknown.

Differentiation of stem cells is correlated with terminal mitosis and cell cycle exit.[43–45] The cyclin A and B are mitotic cyclins that promote the S/M phase entry and the G2/M transition for mammary stem cell division, respectively.[46] Knockdown of cyclin A, cyclin B, cyclin E, or CDKs results in loss of pluripotency and triggers cell differentiation.[47,48] However, the regulatory relationship between cell cycle, epigenetic modification, and differentiation during spheroid formation of ASCs is still unknown. In this study, the subpopulations and gene expression profiles in spheroids derived from ASCs, as well as its cell cycle and reprogramming signaling network that is regulated by epigenetic factors, were investigated. Our finding revealed the interplay between the H3K4me3, H3K9me3, and HDAC5 epigenetic modifiers and their regulatory enzymes (KMT2A and SUV39H1) in promoting the ASCs' reprogramming potential during chitosan-induced spheroid formation.

Materials and Methods

All details pertaining to the chemicals and materials used in this study are shown in Supplementary Table S1. The details of Nuclear/Cytosol fractionation, HATs/HDACs activity assay, Western blotting analysis, RNA extraction and real-time quantitative PCR, and immunofluorescent staining are shown in Supplementary Methods.

Primary Culture of Human Adipose-Derived Stem Cells and Spheroid Induction

Human ASCs, which are human mesenchymal stem cells harvested from normal human adipose tissue, were purchased from Promocell GmBH (C12977). ASCs were cultured in a mixture of 25% mesenchymal stem cell (MSC) growth medium (Gibco) and 75% Dulbecco's modified Eagle's medium high glucose (DMEM-high), supplemented with 10% fetal bovine serum (FBS) and 1% penicillin/streptomycin in a 5% CO_2 humidified incubator at 37 °C. To induce spheroid formation from ASCs, we followed the protocols described in previous studies for the differentiation of neural lineage-like cells (NLCs), a spheroid neural regeneration model, using a chitosan-deposited surface.[17,24,49] Briefly, 1% w/v chitosan acetic acid was coated onto Petri dishes. The nano-deposited dishes were then washed with 1N NaOH solution, PBS, and MQ water. ASCs were seeded onto the chitosan-coated surface at a density of 1×10^6 cells/10 mL for 72 hours to induce spheroid formation. Subsequently, the induced spheroids were harvested for analysis.

Single-Cell RNA Sequencing (scRNA-seq) Assay

Preparation of a Single Cell Suspension

ASCs and spheroids were digested with 0.05% trypsin (Invitrogen) for 1 and 10 minutes, respectively. Subsequently, cells were centrifuged at 500 x *g* for 5 minutes, and the pellets were resuspended in growth media containing 10% FBS. The cell concentration was determined by Countstar (Aber Instruments Ltd). The target cell concentration of 1×10^6 cells per milliliter was achieved by adding appropriate volumes of growth medium with 10% FBS.

Single-Cell RNA-seq Library Preparation and Sequencing

Using the Chromium Next GEM single-cell 3′ v3.1: cell multiplexing protocol (10x Genomics), single cells from ASCs and Spheroids were labeled with Cell Multiplexing Oligos (CMO) for grouping. The labeled cells were loaded onto the 10x Genomics Single Cell Chip G cartridge, where they were encapsulated within droplets containing barcoded gel beads. This process generated single-cell Gel Beads-in-Emulsion (GEMs) and facilitated reverse transcription. Inside the droplets, mRNA capture occurred using a 30 bp oligo-dT after cell lysis. Barcodes (14 bp) were provided to index cells and transcripts (10 bp UMI). Following reverse transcription, the cDNAs tagged with both CMO and UMI barcodes were amplified, and a library was constructed using the Chromium Next GEM Single Cell 3′ Reagent Kits v3.1_Dual Index (10x Genomics). The resulting libraries were sequenced on an Illumina NextSeq 2000 System using a 2 × 150 bp configuration (Illumina, Inc.).

Sample Demultiplexing, Barcode Processing, and UMI Counting

Sample demultiplexing, barcode processing, and UMI counting were performed using the official 10x Genomics pipeline Cell Ranger v3.1.0 (https://support.10xgenomics.com) (10X Genomics). Raw base call files generated by Illumina sequencers were demultiplexed into reads in FASTQ format using the "cellranger mkfastq" pipeline. The raw reads

were trimmed from the 3′ end to obtain the recommended number of cycles for read pairs (Read1: 26 bp; Read2: 98 bp). The reads from each library were then processed separately using the "cellranger count" pipeline to generate a gene-barcode matrix for each library. During this step, the reads were aligned to a human reference genome (version: GRCh38-3.0.0). Cell barcodes and UMIs associated with the aligned reads were corrected and filtered. As a parameter related to cell barcode filtering, the expected number of recovered cells was set to 8000 in this study.

Dimensional Reduction, Clustering, and UMAP Projection

Based on expression and dispersion, we selected 1889 highly variable genes ($\log_2$FC threshold = 0.25). The data on these genes were then subjected to dimensional reduction through principal component analysis (PCA). We used the first 30 principal components to cluster the cells into subpopulations using a graph-based unsupervised clustering approach implemented in Seurat v5. This approach utilizes clustering algorithms to group cells with similar gene expression profiles into distinct clusters. These clusters can then be annotated or labeled based on known cell type markers, allowing for the identification of different cell types or subpopulations within the dataset. After the clustering step, the same principal components obtained from the clustering analysis were used to project the clustered cells onto a two-dimensional (2D) map. To achieve this projection, we used the Uniform Manifold Approximation and Projection (UMAP) technique, a robust method for reducing the dimensionality of high-dimensional data. UMAP effectively captures the local structure of the data and maps it onto a lower-dimensional space, facilitating clear visualization of relationships and patterns among the clustered cells.

Gene Set Enrichment Analysis and Pathway Analysis

Genes with $\log_2$FC ≥ 0.5 or $\log_2$FC ≤ −0.5 and *P*-value < .05 were selected for further analysis. To explore cell fate and cluster associations, Monocle 2 software[50] was used for trajectory analysis, cross-analyzing cell differentiation trajectories between clusters from ASCs and spheroids. Additionally, Ingenuity Pathway Analysis (IPA, QIAGEN Inc.) software was used for gene expression pattern analysis, canonical pathways, and directional predictions.

Statistical Analysis

Statistical analysis was performed using Prism 8 software (GraphPad, La Jolla). A *P*-value < .05 was considered statistically significant in this study. The specific statistical methods for each figure were indicated in the respective figure legends.

Results

Spheroid Formation Arrests the Cell Cycle and Increases Epigenetic Regulations

During stem cell differentiation, the timing of terminal mitosis and cell cycle exit is closely linked, and this process is associated with a decrease in the expression of cell cycle markers, including cyclin A and cyclin B.[44] In the specific context of chitosan-induced spheroid formation, the expression of cyclin A1 and cyclin B1 was found to be reduced within 16 hours and sustained at a low level for 72 hours in spheroids compared to the regular culture of ASCs (Fig. 1A; quantification results were shown in Supplementary Fig. S1A).

Chromatin regulation drives stem cell pluripotency, differentiation, and cell-type-specific gene expression through dynamic changes in histone trimethylation. Given that the N-terminal domains of histones are highly associated with histone modifications in stem cells, we measured the histone trimethylation of H3 in ASCs and its differentiated spheroids using western blotting of H3K4me3, H3K9me3, and H3K27me3. The spheroids showed significant increases in H3K4me3, H3K9me3, and H3K27me3 soon after seeding ASCs on the chitosan-coated surface for spheroid formation (Fig. 1B; quantification results were shown in Supplementary Fig. S1B). In addition, histone acetylation and/or deacetylation were further analyzed using HAT and HDAC enzymatic activities assays, respectively. Compared to the increases of HAT activities in ASCs during different time points of cell culture, a decrease in HAT activity was observed at 72 hours after spheroid induction (Fig. 1C). The reduction of HAT at 72 hours agreed with the cell cycle arrest protein expressions shown in Fig. 1A during spheroid formation. Interestingly, the HDAC activities were increased at 16 hours and maintained at high activity levels during spheroid induction (Fig.1D).

We further dissected the expression profiles of Class I and IIa HDACs using whole-cell lysates for western blotting. The expressions of Class I HDACs (HDAC1, HDAC2, and HDAC3) showed no differences between ASCs and spheroids (Fig. 1E; quantification results were shown in Supplementary Fig. S1C). However, the Class IIa HDACs, particularly the HDAC5 and p-HDAC4/5/7 were significantly increased during spheroids formation (Fig. 1E, Supplementary Fig. S1C). Since Class IIa HDACs are a group of transcriptional regulators and can shuttle between cytoplasm and nucleus, we further examined the subcellular localization of HDAC5. Immunofluorescent staining (IF) of HDAC5 showed translocation of HDAC5 into the nuclear in spheroids (Fig. 1F; quantification results were shown in Supplementary Fig. S1D). Immunoblotting of cytosolic and nucleus proteins confirmed the HDAC5 translocated into the nucleus at 48 and 72 hours after induction, whereas other Class II HDAC of HDAC4 and pHDAC4/5/7 remained in the cytosol (Fig. 1G; quantification results were shown in Supplementary Fig. S1E). After nucleus translocation, the HDAC5 activity in the cell nucleus was significantly increased in spheroids (Fig. 1H). These results suggested that chitosan-induced ASCs spheroid formation exhibits the characteristics of cell cycle arrest and highly epigenetic modifications for potential stem cell reprogramming and/or differentiation.

Single-Cell RNA Sequencing Identified Distinct Subpopulations in Spheroids

To reveal detailed stem-cell information and characteristics during ASCs spheroid formation on the chitosan surface, scRNA-seq libraries of ASCs and spheroids were analyzed using the 10x Genomics 3′ CellPlex multiplexing platform. The scRNA-seq process involved dissociating ASCs and spheroids into individual single cells and included procedures for encapsulating, labeling, and sequencing (Fig. 2A). The cells from ASCs and spheroids were visualized in a 2D UMAP plot, clearly showing 2 distinct groups of cells (Fig. 2B). The cells were further clustered into 8 subpopulations using a shared nearest neighbor (SNN) modularity optimization-based clustering algorithm with a resolution of 0.45 (Fig. 2C). The

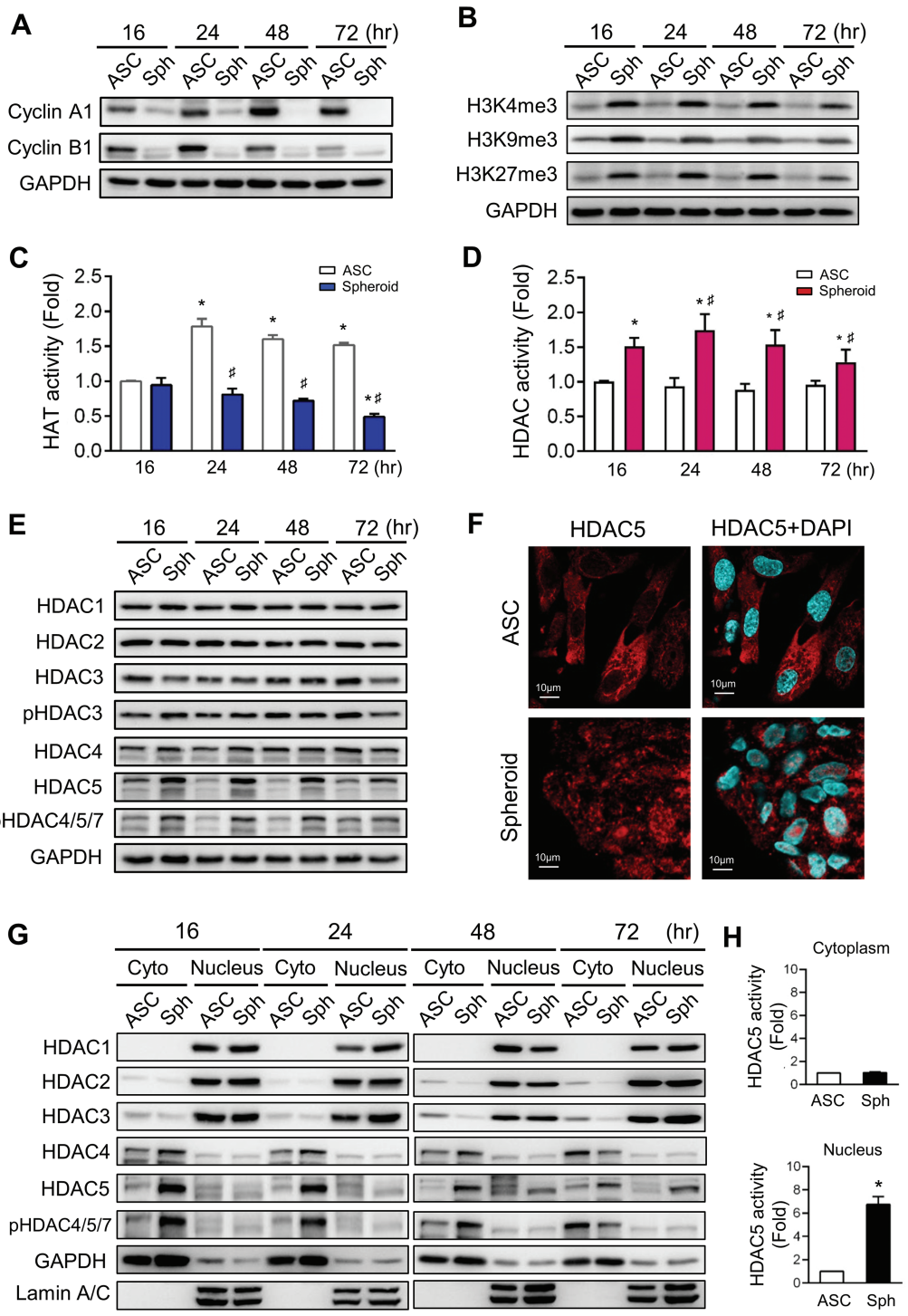

Figure 1. Cell cycle arrest and epigenetic regulations during spheroid formation of ASCs. (**A**) Representative western blotting analysis of cyclin A1 and B1 expressions in chitosan-induced spheroids (Sph) from ASCs (control) after different time points of 16, 24, 48, and 72 hours induction. (**B**) Western blotting analysis of H3K4me3, H3K9me3, and H3K27me3 expressions in chitosan-induced Sph at different time points. (**C**, **D**) Comparison of HATs activities (C) and HDACs activities (D) in Sph after spheroid formation. (**E**)Western blotting analysis of HDAC1, HDAC2, HDAC3, p-HDAC3, HDAC4, HDAC5, and p-HDAC4/5/7 expressions in Sph after 16-72 hours of induction. (**F**) Representative confocal immunofluorescence images of ASCs and spheroids stained with anti-HDAC5 antibody and DAPI. (**G**) Representative western blotting expressions of HDACs in cellular and nuclear extracts from spheroids. GAPDH and Lamin A/C were used as markers and loading controls for cytoplasm and nucleus, respectively. (**H**) HDAC5 activities in cytoplasm and nucleus of spheroids after 72 hours of chitosan induction. Data in bar graphs represent mean ± SEM of at least 3 independent repeats and were analyzed by 2-way ANOVA with Sidak's multiple comparisons post-test in (C) and (D). Data in (H) were analyzed by Student's *t* test. $^{*}P < .05$ and $^{**}P < .001$ versus the ASC control group at 16 hours. $^{\sharp}P < .05$ and $^{\sharp\sharp}P < .001$ versus the ASC control group at each time point. Quantification and statistical analysis of Western blot assays in (A), (B), (E), (G), and HDAC5-nuclear translocated cells within confocal images in (F), are shown in Supplementary Fig. S1.

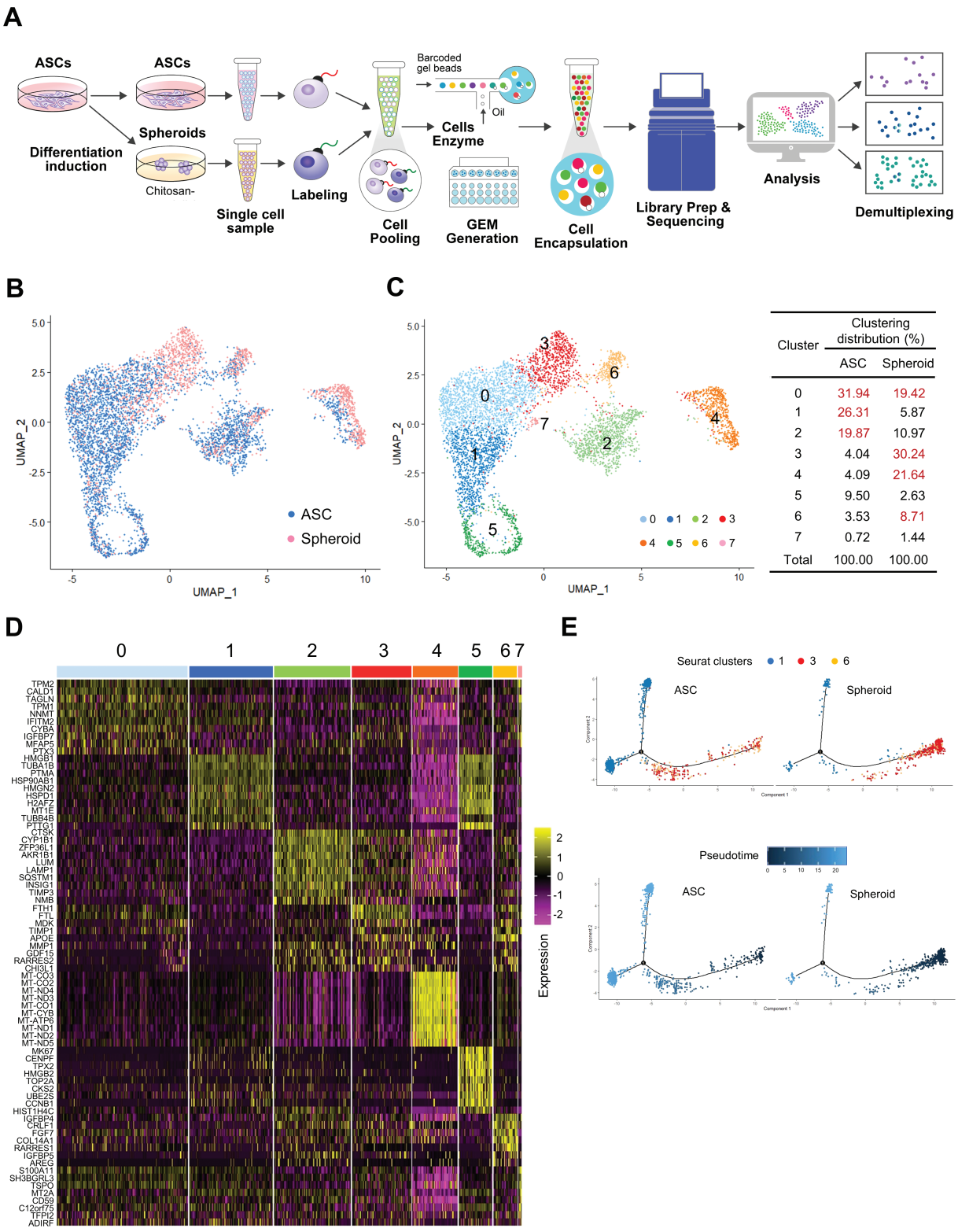

Cluster	Clustering distribution (%)	
	ASC	Spheroid
0	31.94	19.42
1	26.31	5.87
2	19.87	10.97
3	4.04	30.24
4	4.09	21.64
5	9.50	2.63
6	3.53	8.71
7	0.72	1.44
Total	100.00	100.00

Figure 2. Single-cell RNA-sequencing reveals different cell subpopulations and gene profiles of chitosan-induced spheroids and ASCs. (**A**) Workflow of single-cell RNA-sequencing experiments and analysis. (**B**) Distribution of cells from ASCs and spheroids in a 2D UMAP plot. (**C**) 2D UMAP plot showing 8 color-coded clusters of ASCs and spheroids. The right panel indicates the percentage distribution of clusters in ASCs and spheroids. (**D**) Heat map displaying the top 10 genes with the highest average $\log_2$ fold change of each cluster. (**E**) Single-cell trajectory analysis using Monocle 2 software. The top 300 genes with the highest expression were used to construct the pseudotime tree. Cells on the tree are colored by Seurat cluster assignment (upper panel). In the lower panel, the arrangement of trajectory inference shows that cells on the left side of the tree are less differentiated than those on the right side.

detailed percentages of cells in each cluster were listed, with ASCs showing significant proportion in Cluster 0 (31.94%), 1 (26.31%), 2 (19.87%), and 5 (9.5%). Spheroids exhibited major subpopulations in Cluster 0 (19.42%), 2 (10.97%), 3 (30.24%), 4 (21.64%), and 6 (8.71%). The top 20–30 genes (fold change > 1.5, $\log_2$ FC > 0.58) for each cluster are listed in Supplementary Table S4. The heatmap highlights the expression levels of the top 10 genes in each cluster, emphasizing differentially expressed gene profiles (Fig. 2D).

Cell fate trajectory analysis revealed the transition of ASCs to spheroids at single-cell resolution, displaying a continuum of cells leading to one branch point and three distinct fates. Cluster 1 cells in ASCs were found at two distinct ends of the trajectory, while Cluster 3 cells in spheroids were located at the third end. Cluster 6 cells were positioned between the branch point and the Cluster 3 end (Fig. 2E, upper panel). Overlaying of cluster trajectory distribution with the pseudotime tree map indicated that Cluster 3 cells in spheroids differentiated from Cluster 1 cells in ASCs (Fig. 2E, lower panel). Cluster 6 cells aligned with the trajectory fate of Cluster 3 but did not reach the trajectory end of cell fate. Furthermore, several genes in Cluster 6 cells were associated with the gene profile of Cluster 3 (Supplementary Table S4). These results suggested a transient subpopulation of Cluster 6 cells shifting toward the Cluster 3 cell lineage during chitosan-induced ASCs spheroid formation. In addition to the cell fate association among Clusters 1, 3, and 6 in ASCs and spheroids, another association was observed between Clusters 0 and 4, which is highly associated with mitochondria function between ASCs and spheroids (this will be reported in a separated paper). Together, the scRNA-seq results provided detail information confirming the presence of multiple populations, particularly the gene profile related to neuronal lineage differentiation, during the spheroid formation of ASCs on the chitosan-coated surface.

Identification of Potential Targets on Epigenetic Regulations in Clusters 3 and 6 Cells

The epigenetic regulatory mechanism was investigated by integrating the scRNA-seq gene profiling, histone trimethylation, and HDAC5 into the IPA software. Prior to network association, the specificity of gene expression in Clusters 6 and 3 cells was confirmed by superimposing the expression levels among different subpopulations. Specifically, for Cluster 6 cells (red circle population), the *retinoic acid receptor responder 1 (RARRES1)*, *amphiregulin (AREG)*, *IFG binding protein 5 (IGFBP5)*, *FGF7*, *and prostaglandin E Synthase (PTGES), transglutaminase 2 (TGM2)* were identified as the major upregulated genes among the top 30 genes on UMAP (Fig. 3A). *RARRES2*, *midkine (MDK)*, *growth differentiation factor 15 (GDF15)*, *glycoprotein non-metastatic gene B (GPNMB)*, *cathepsin K (CTSK)*, *and cellular communication network factor 5 (CCN5)* were highly expressed specifically in Cluster 3 cells (Fig. 3B, red diamond population). Some genes, including *apolipoprotein E (APOE)*, *serpin family F member 1 (SERPINF1)*, *dual specificity phosphatase 1 (DUSP1)*, *SRY-Box transcription factor 4 (SOX4)*, *superoxide dismutase 2 (SOD2)*, *chitinase 3 Like 1 (CHI3L1)*, *and microfibril-associated glycoprotein 4 (MFAP4)*, were expressed in both Clusters 6 and 3 cells (Fig. 3C, red rectangle populations).

Using the IPA software, potential regulatory pathways were explored by connecting histone methylation enzymes, HDAC5, and the aforementioned target genes specifically expressed in Cluster 3 and/or 6, using the IPA molecule activity predictor (IPA-MAP tool). This allowed us to predict the activated and inhibited effects of the signaling pathways for stem cell reprogramming potential and linage differentiation during ASCs spheroid formation. In Cluster 6, the major upregulated genes were found to be downstream signals close to KMT2A, SUV29H1, and EZH2, which are specific histone methyltransferases (HMTs) for H3K4me3, H3K9me3, and H3K27me3, respectively. Additionally, HDAC5, a histone deacetylase, was also identified. (Fig. 4A). From the IPA-MAP tool, the major upregulated genes predicted for Cluster 6 cells during spheroid induction included the *homeobox genes (HOX) family (HOXA7*, *HOXB5*, *HOXB6 and HOXB7)*, *sclerostin (SOST)*, *high mobility group AT-Hook 2 (HMGA2)*, *neurogenin-1 (NEUROG1)*, *cyclin-dependent kinase inhibitor 1 (CDKN1A)*, *FGF7*, *RARRES1 IGFBP4*, *IGFBP5*, *PTGES*, *and SERPINF1*. The major signals associated with the transient subpopulation of Cluster 6 were linked to KMT2A and SUV29H1 (Fig. 4A). In Cluster 3, the major predicted genes in the network were *GDF15*, *MDK*, *CTSK*, *GPNMB*, *CCN5*, *RARRES2*, *NEUROG1*, *MFAP4*, *tumor protein p53 (TP53)*, *nuclear protein 1 (NUPR1)*, *matrix metallopeptidase 1 (MMP1)* (Fig. 4B). The major predicted signals in Cluster 3 shifted toward differentiated cells and/or reprogramming factors, indicating a late-stage subpopulation compared to the transient cell status in Cluster 6. This finding agreed with the cell fate trajectory analysis of Clusters 1, 3, and 6 in Fig. 2E. To further confirm the predicted signaling network in spheroids, we measured the expression of these target genes using qPCR analysis and showed the mean fold change on each gene in spheroids compared to ASCs (Fig. 4C; the relative fold changes represented in the bar chart are shown in Supplementary Figs. S2–S8). Although the qPCR results measured the whole population of spheroids, increases in these target genes were still observed after seeding ASCs on a chitosan-coated surface for 72 hours.

H3K4me3 and H3K9me3 Played a Dominant Role in Reprogramming and Differentiation of ASC-Derived Spheroids

To further validate the role of epigenomic regulators, specifically histone trimethylation at H3K4, H3K9, and H3K27, as well as the HDAC5, we used specific inhibitors to investigate their involvement in these upregulated genes and pathways during spheroid formation. The inhibitor SNDX-5613, which targets KMT2A (MLL1) and is also known as Revumenib, was used to decrease MLL1 chromatin binding by disrupting the interaction between MLL1 and Menin, thereby reducing the enzymatic product of KMT2A on H3K4me3. We used the SUV39H1 inhibitor Chateocin (SUVi) to specifically block the H3K9me3, which is catalyzed by SUV39H1, the human homolog of the Drosophila Su(var)3-9 histone methyltransferase. GSK126 was used to inhibit EZH2, responsible for H3K27me3, and LMK235, an HDAC5 inhibitor, was used to study the role of HDAC5 on the identified genes and pathways in Clusters 3 and 6. The effects of different inhibitors were summarized as relative fold changes in gene expression compared to spheroids without inhibitors (Table 1). Relative gene fold changes are shown in Supplementary Figs. S2–S8 after testing at varying dosages during spheroid formation (Supplementary Figs. S9–S12).

The qPCR results revealed that in the Cluster 6 subpopulation, the expression of HOX family genes (such as

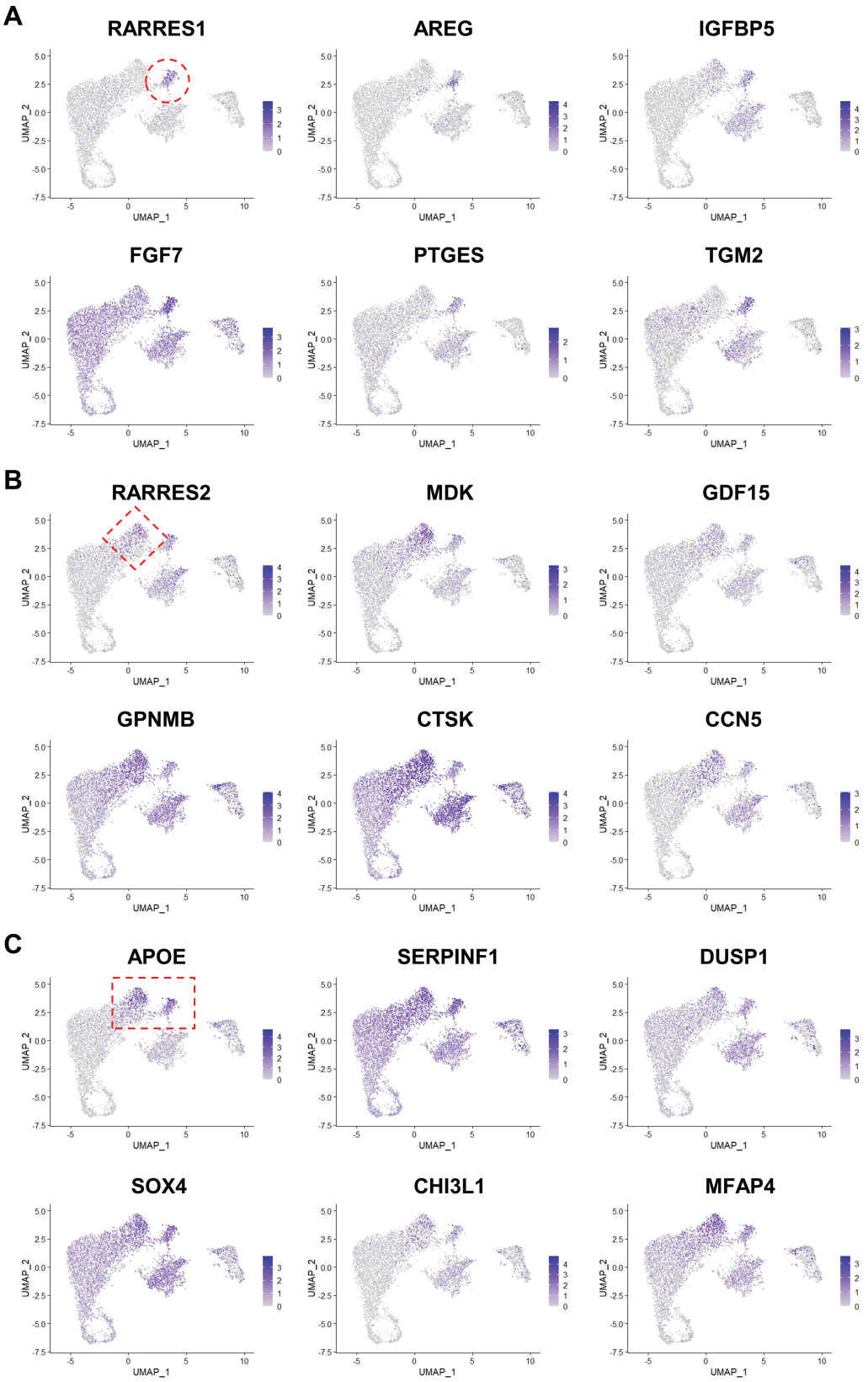

Figure 3. Expression and distribution map of top genes in Clusters 3 and 6. Genes highly and specifically expressed in (**A**) Cluster 6, (**B**) Cluster 3, and (**C**) both Clusters 3 and 6 after spheroid formation are overlaid in the 2D UMAP plot.

HOXA7, HOXB5, HOXB6, and HOXB7), known as driving factors in stem cell differentiation, as well as genes specifically expressed in Cluster 6 (such as *IGFBP4*, *IGFBP5*, *RARRES1*, *FGF7*, and *PTGES*), were significantly inhibited by 70 μM SNDX-5613 and 25 nM SUVi, respectively (Table 1, Cluster 6 genes; relative gene fold changes are shown in Supplementary

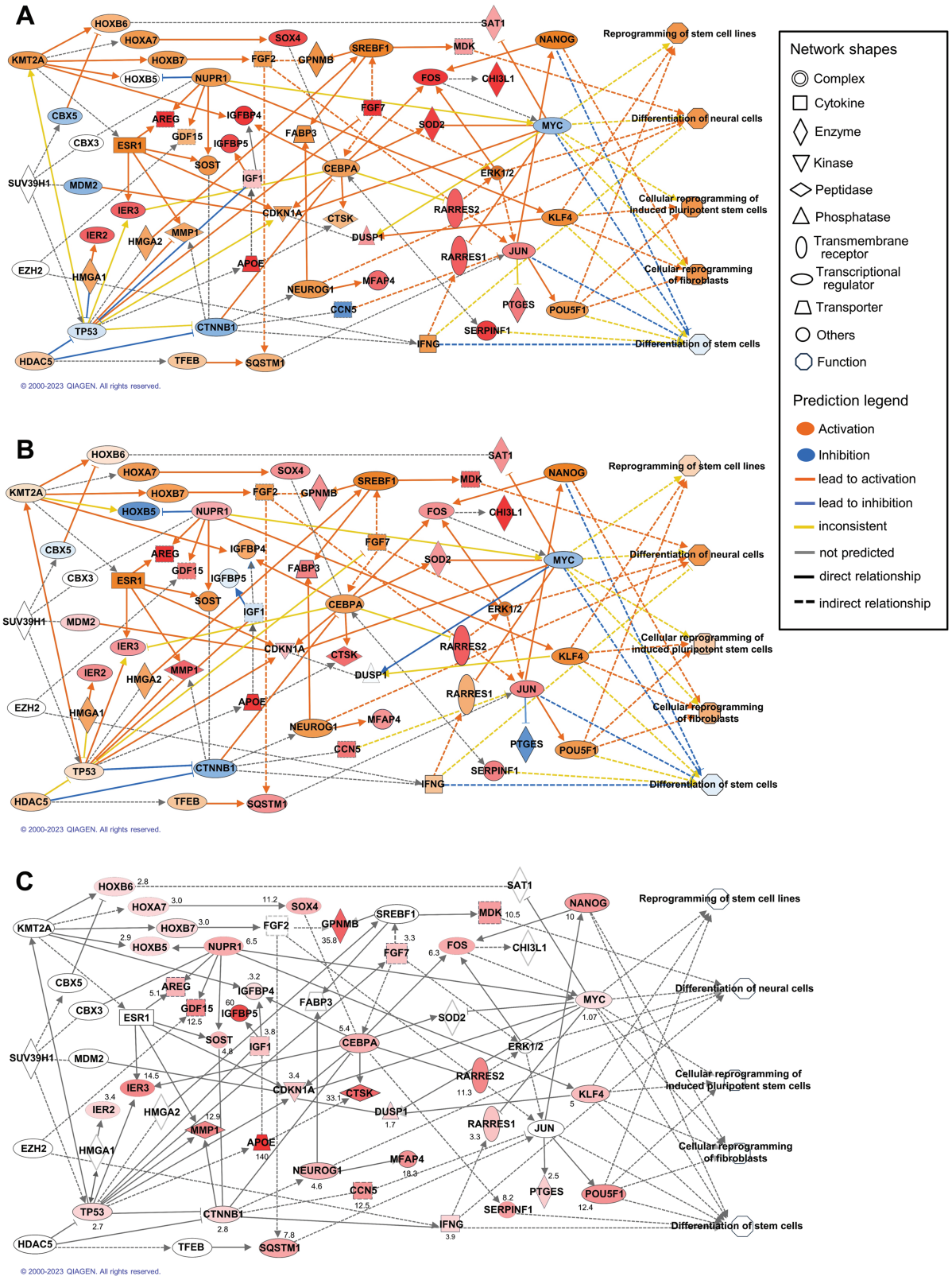

Figure 4. Interactive network of histone modification enzymes and differentially expressed genes. IPA prediction of the interactive network between the histone H3 modification enzymes and differentially expressed genes in transient subpopulation of cluster 6 (**A**) and late-stage subpopulation of cluster 3 (**B**). The Network is overlaid with the scRNA-seq gene expression dataset of clusters 6 and 3 using the IPA-MAP tool to predict the activation/inhibition state of signal pathways. (**C**) Network mapped with qPCR results of relative gene expressions as compared spheroids to ASCs. Numbers next to the molecules represent the fold change.

Table 1. Gene expression profiles in response to inhibition treatment.

Genes	Inhibitor of KMT2A (SNDX-5613)	Inhibitor of SUV39H1 (Chaetocin)	Inhibitor of EZH2 (GSK126)	Inhibitor of HDAC5 (LMK235)
Cluster 6 genes				
RARRES1	0.27 ± 0.04**	1.11 ± 0.10	0.15 ± 0.03**	0.54 ± 0.01*
AREG	0.64 ± 0.04*	0.68 ± 0.05*	1.16 ± 0.30	2.25 ± 0.30*
IGFBP5	0.15 ± 0.07**	0.12 ± 0.06**	0.26 ± 0.06**	0.52 ± 0.05**
IGFBP4	0.49 ± 0.08**	0.33 ± 0.08**	0.72 ± 0.09	0.69 ± 0.09
FGF7	0.69 ± 0.08**	0.77 ± 0.03**	1.36 ± 0.14	1.09 ± 0.03
PTGES	0.61 ± 0.07*	3.42 ± 0.43**	3.36 ± 1.12*	1.37 ± 0.12**
HOXA7	0.40 ± 0.08**	0.42 ± 0.04**	1.02 ± 0.07	1.12 ± 0.12
HOXB5	0.71 ± 0.10*	0.48 ± 0.05**	1.10 ± 0.02	0.86 ± 0.13
HOXB6	0.55 ± 0.05*	0.55 ± 0.05*	1.18 ± 0.03	1.04 ± 0.08
HOXB7	0.60 ± 0.06*	0.41 ± 0.03**	1.00 ± 0.04	0.85 ± 0.05
Cluster 3 genes				
RARRES2	0.63 ± 0.06*	0.23 ± 0.11**	0.67 ± 0.08*	0.68 ± 0.10*
MDK	0.34 ± 0.11*	0.42 ± 0.03*	1.07 ± 0.28	1.07 ± 0.21
GDF15	0.48 ± 0.06*	0.45 ± 0.05*	1.39 ± 0.30	1.50 ± 0.32
GPNMB	0.58 ± 0.08*	0.31 ± 0.05**	1.14 ± 0.04	0.55 ± 0.09*
CTSK	0.33 ± 0.02**	0.21 ± 0.02**	1.23 ± 0.16	0.43 ± 0.11**
CCN5	0.62 ± 0.02*	0.15 ± 0.02**	0.96 ± 0.15	0.36 ± 0.07**
Clusters 6 and 3 genes				
APOE	0.67 ± 0.10*	1.37 ± 0.17	1.19 ± 0.07	3.05 ± 0.44
DUSP1	0.55 ± 0.06*	1.30 ± 0.10	1.83 ± 0.19	1.13 ± 0.05
SERPINF1	0.43 ± 0.05*	0.16 ± 0.02**	0.89 ± 0.14	0.44 ± 0.15*
SOX4	0.67 ± 0.04*	0.36 ± 0.01**	1.15 ± 0.06	0.40 ± 0.04**
MFAP4	0.95 ± 0.19	0.02 ± 0.01**	0.70 ± 0.16*	0.13 ± 0.07**
NEUROG1	0.60 ± 0.05*	0.44 ± 0.13**	0.88 ± 0.18	1.42 ± 0.15
NUPR1	0.61 ± 0.10**	0.14 ± 0.06**	0.98 ± 0.12	0.34 ± 0.05**
SOST	0.46 ± 0.12**	1.16 ± 0.14	1.30 ± 0.32	1.22 ± 0.30
IER2	0.68 ± 0.13*	0.46 ± 0.08*	1.02 ± 0.13	1.16 ± 0.02
IER3	0.48 ± 0.08*	1.58 ± 0.36	1.29 ± 0.30	1.01 ± 0.12
FOS	1.02 ± 0.03	1.00 ± 0.05	0.47 ± 0.02**	1.55 ± 0.79
IPA predicted regulator				
TP53	0.53 ± 0.13*	0.56 ± 0.08*	0.85 ± 0.05	0.65 ± 0.08*
CYP1B1	0.34 ± 0.05**	0.56 ± 0.07*	1.07 ± 0.05	0.89 ± 0.09
IGF1	0.33 ± 0.14**	0.29 ± 0.23**	0.81 ± 0.09	0.82 ± 0.09
IFNG	0.61 ± 0.11*	0.62 ± 0.13*	0.87 ± 0.11	0.98 ± 0.08
CDKN1A	0.48 ± 0.03**	0.55 ± 0.09*	0.75 ± 0.05*	1.45 ± 0.19
Neural lineage markers				
NR2E1	0.60 ± 0.14*	0.52 ± 0.08*	0.97 ± 0.16	1.10 ± 0.03
ADRA1A	0.48 ± 0.10*	0.45 ± 0.04**	0.91 ± 0.24	0.90 ± 0.10
ADRA1B	0.49 ± 0.11*	0.41 ± 0.03**	0.81 ± 0.05	0.83 ± 0.03
Yamanaka factors				
OCT4	0.27 ± 0.07**	0.38 ± 0.06**	1.24 ± 0.28	1.18 ± 0.10
SOX2	0.65 ± 0.13*	0.34 ± 0.06**	1.10 ± 0.17	1.15 ± 0.04
KLF4	0.75 ± 0.02*	0.26 ± 0.07**	1.11 ± 0.19	1.12 ± 0.11
MYC	1.00 ± 0.05	0.34 ± 0.08**	0.83 ± 0.17	0.74 ± 0.08
Nanog	0.26 ± 0.03**	0.44 ± 0.06**	1.37 ± 0.38	1.33 ± 0.08

This table summarizes the gene expression profiles of Clusters 3 and 6 genes from scRNA-seq analysis, along with the IPA predicted genes observed following the inhibition of KMT2A, SUV39H1, and EZH2 for the HMTs responsible for trimethylation at H3K9, H3K4, and H3K27, respectively. The inhibitions were achieved by treating 70 μM SNDX-5613 (KMT2A inhibitor), 25 nM SUVi (SUV39H1 inhibitor), and 10 μM GSK126 (EZH2 inhibitor) during spheroid formation. The 500 nM LMK235 was applied to inhibit the HDAC5 expression and activity. The value represents fold change in inhibitor-treated group divided by the spheroid treated with vehicle control. All data are represented as the mean ± SEM of at least 3 independent repeats and analyzed by Student's *t* test. $^{*}P < .05$, and $^{**}P < .001$ versus the spheroid. The corresponding bar chart figures are shown in Supplementary Figs. S2–S8. Red color indicates decreased numbers.

Fig. S2). This suggests that KMT2A (H3K4me3) and SUV39H1 (H3K9me3) are involved in the differentiation process within the Cluster 6 subgroup. In contrast, EZH2 (H3K27me3) and HDAC5 showed less significant regulation of gene expression and had a lesser impact on the differentiation potential in this specific transient subpopulation. Although both H3K4me3 and H3K9me3 enzyme inhibitors exhibited inhibitory effects on many stem cell potency and differentiation genes, slight differences were observed between the SNDX-5613 (KMT2A inhibitor) and the SUVi (SUV39H1 inhibitor). For instance, the RARRES1 and PTGES were only inhibited by blocking the KMT2A signaling on H3K4me3, not by the SUVi for SUV39H1 inhibition on H3K9me3 (Table 1, Cluster 6 genes). On the other hand, the regulation of stem cell potential and lineage in Cluster 3 cells was primarily influenced by KMT2A (H3K4me3), SUV39H1 (H3K9me3), and HDAC5 (Table 1, Cluster 3 genes; relative gene fold changes are shown in Supplementary Fig. S3). Certain genes in Cluster 3, such as CTSK, GPNMB, and CCN5, were inhibited by SUVi (H3K9me3) and HDAC5 inhibitor, but not by the KMT2A (H3K4me4) inhibitor. This indicates that the translocation of HDAC5 into the nucleus during spheroid formation is more involved in Cluster 3 gene regulation. The trimethylation at H3K9 has more impact than trimethylation at H3K4 in the endpoint state spheroid subpopulation. In genes expressed in both Clusters 3 and 6 cells, the major regulatory mechanism shifted to H3K9me3 and HDAC5 (Table 1, Clusters 3 and 6 genes; relative gene fold changes are shown in Supplementary Fig. S4). These findings emphasize the potential importance of epigenetic regulation, particularly H3K4me3, H3K9me3, and HDAC5, in shaping the differentiation potential of cells and directing their commitment to specific lineages.

Cross-Talk Between Epigenetic Regulators and Spatial Distribution of Subpopulations

To confirm the spatial distribution of Clusters 3 and 6 cells in the subpopulations of spheroids, we used the GFAP and KMT2A as demonstrated by superimposing cluster target gene (Fig. 3) to represent the cells of Clusters 6 and 3, respectively (Fig. 5A). The immunofluorescent staining was performed by labeling the positive staining of GFAP (FITC, green color) and KMT2A (TRITC, red color) in spheroids. The co-localization of KMT2A and GFAP suggested the driving force of H3K4me3 to facilitate the stem-cell potential and differentiate toward glia-positive precursor cells during spheroid formation. The trimethylation of H3K9me3 was also confirmed by FRET reporter assay of H3K9me3 using FRET confocal microscopy. The FRET activation image exhibited a distribution in the central core of the spheroid, indicating the region of H3K9me3 (Supplementary Fig. S13).

To further investigate the potential interaction of these inhibitors, we performed Western blotting assays to study the specificity and potential crosstalk between the different inhibitors. The SNDX-5613 effectively inhibited the trimethylation of H3K4 and H3K9 but had no effect on H3K27me3, HDAC5, and pHDAC4/5/7 (Fig. 5B; quantification results are shown in Supplementary Fig. S14A). The SUV39H1 inhibitor chaetocin (SUVi) not only inhibited the H3K9me3 but also inhibited the levels of H3K4me3 and H3K27me3 (Fig. 5C; quantification results were shown in Supplementary Fig. S14B). Furthermore, SUVi inhibited both the expression of HDAC5 (Fig. 5C) and the nuclear translocation of HDAC5 (Supplementary Fig. S15). Both SNDX-5613 and SUVi inhibited the expression of KMT2A and abolished the differentiation as illustrated by no expression of GFAP during spheroids formation (Fig. 5D). These findings provide additional insight into epigenetic regulation into the spatial distribution of these subpopulations within the spheroid structure.

Discussion

Our results highlight the critical roles of epigenetic regulation, specifically H3K4me3 (KMT2A) and H3K9me3 (SUV39H1), in Cluster 6 during the transient state of spheroid formation (Graphical Abstract). Moreover, H3K9me3 and HDAC5 play major regulatory roles in Cluster 3, corresponding to the end stage of spheroid formation and neural differentiation in ASCs. The unique gene expression patterns observed in Cluster 6 (RA, RARRES1, IGF, PTGES, and FGF7) and Cluster 3 (GDF15, MDK, GPNMB, RARRES2) potentially enhance the sensitivity of spheroids toward cellular fate determination and differentiation signals. Notably, genes highly upregulated in both Clusters 3 and 6, such as APOE, NUPPR1, DUSP1, NEUROG1, and SOX4, are associated with neural differentiation (Graphical Abstract), highlighting the significance of these clusters in promoting neural lineage commitment. However, HDAC5 inhibitor LMK235 showed less significant regulation of gene expression in Cluster 6 cells and was more associated with the differentiation of the endpoint state of Cluster 3 cells. These results suggest the HDAC5 translocation from the cytoplasm to the nucleus may later phase differentiation in ASCs spheroids.

Among these orchestrating inductions in Clusters 6 and 3, numerous growth factors and signaling activations of receptors were identified as contributors to stem cell potential and differentiation. For instance, FGF7, which exhibited high expression in Cluster 6 in our current study, has been reported to play a crucial role in cell reprogramming (Figs. 3A and 4A). It facilitates the conversion of differentiated cells into induced pluripotent stem cells (iPSCs) and other reprogrammed cell types by promoting mesenchymal-to-epithelial transition.[51–53] FGF7 interacts with FGFR2, initiating a signaling cascade that alters cell morphology, gene expression, and cellular properties, enabling reprogramming and the acquisition of self-renewal and differentiation abilities.[53] Previous findings of our research demonstrated increased expression of FGFR2 and FGFR4 during spheroid induction,[17] suggesting their potential involvement in FGF7-mediated spheroid processes, potentially through activation of the FGFR2 or FGFR4 signaling pathways. Another important component in stem cells is PTGES (prostaglandin E synthase), which is responsible for producing PGE2. PGE2 is crucial for enhancing the pluripotency factors OCT4, SOX2, and Nanog via cAMP-PKA and Wnt/β-catenin signaling to promote stem cell self-renewal and help maintain their undifferentiated state.[54] It also facilitates the early phase embryonic development and implantation of a fertilized egg.[55] In this study, we observed high expression of PTGES in Cluster 6 (Figs. 3A and 4A), and its expression was regulated by H3K4me3 (Table 1), suggesting the potential role in enhancing reprogramming and stemness potential during spheroid formation.

Regarding neuronal lineage differentiation on chitosan-coated surface, we revealed several potentials signaling factors during ASCs spheroid formation. RARRES1 and RARES2 are genes that respond to retinoic acid (RA) signaling, which

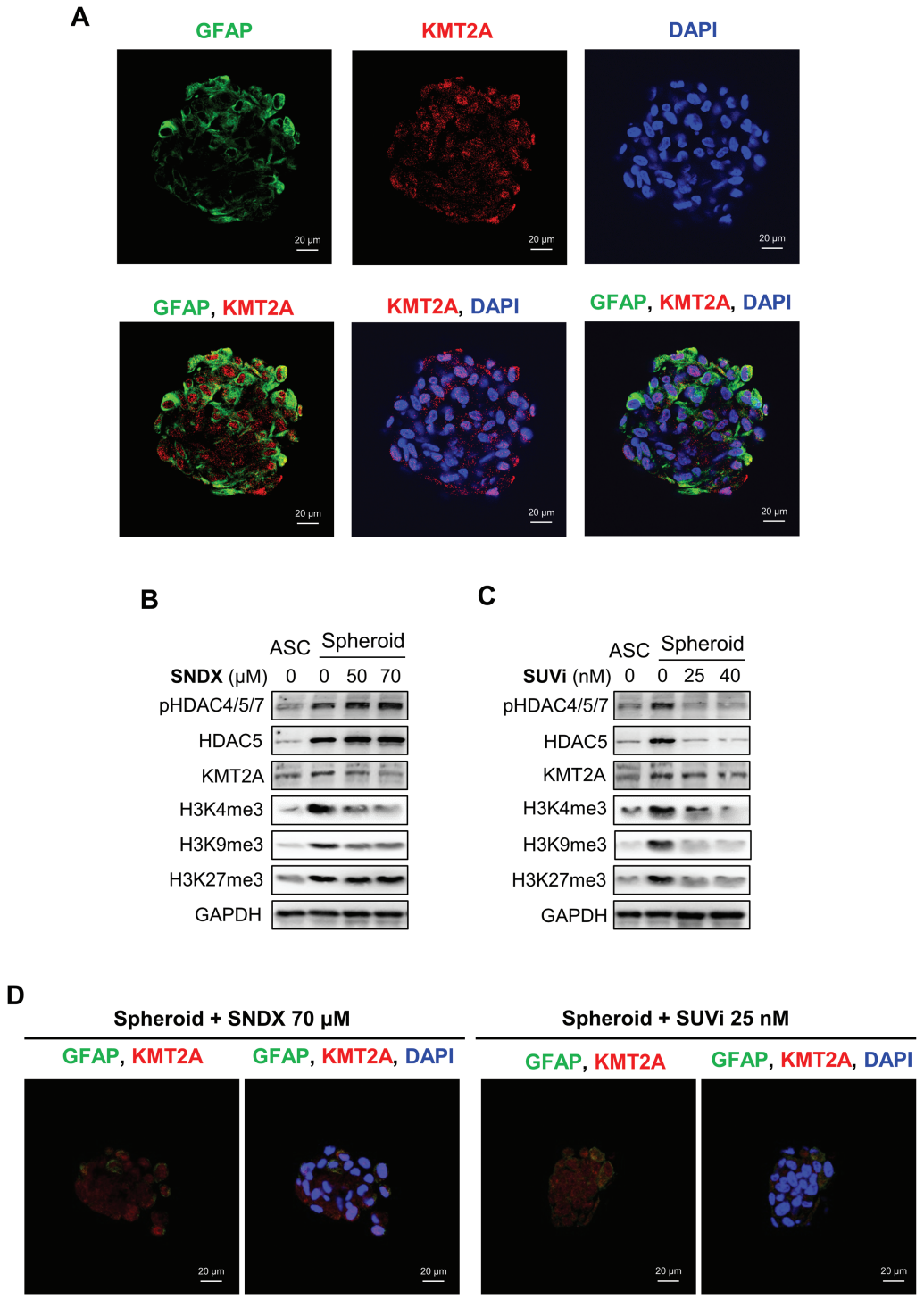

Figure 5. Inhibition of epigenetic regulators and spatial distribution of subpopulation in spheroids. (**A**) Confocal microscope images of immunofluorescent staining for GFAP-KMT2A. Nuclei were stained with DAPI. (**B**, **C**) Interactions between inhibitors of epigenetic regulators were shown in Western blotting analysis by inhibiting the histone methyltransferases of H3K4me3 and H3K9me3 using SNDX-5613 (B) and SUVi (C). (**D**) Representative immunofluorescence images of spheroids treated with SNDX-5613 or SUVi and stained with anti-GFAP, anti-KMT2A , and DAPI. Magnification 60×. All experiments were repeated at least 3 times as independent replicates.

is involved in the differentiation of stem cells into specific lineages (Figs. 3A, 3B, 4A, and 4B). RA acts dually in stem cell differentiation, promoting differentiation by binding to retinoic acid receptors that form complexes with retinoid X receptors (RXRs) and bind to retinoic acid response elements in the nucleus.[56,57] However, short-term exposure to RA inhibits differentiation and sustains pluripotency in human iPSCs.[58] RARRES1 is critical for maintaining pluripotency and preventing differentiation through interactions with epigenetic modifiers. Dysregulation of RARRES1 can affect stem cell fate decisions and differentiation.[59] On the other hand, RARRES2, a lineage-specific transcription factor, exhibits high expression in dormant neural stem cells during differentiation into neural and glial cell fates[60] and in pancreatic

development from pluripotent stem cells.[61] Our findings of RARRES1 in Cluster 6 and RARRES2 in Cluster 3 indicate specific expression patterns and coordination between these two subpopulations of cells. Additionally, the increased expression of RARRES1 was predominantly inhibited by an H3K4me3 inhibitor, while the increased expression of RARRES2 was inhibited by an H3K9me3 inhibitor (Table 1), further suggesting their distinct roles in transient reprogramming and specific lineage guidance of later-stage cells through different H3 trimethylation regulators.

In Cluster 3, highly expressed genes such as GDF15, MDK, and GPNMB, along with RARRES2, are considered differentiation factors involved in cell-fate specification (Fig. 3B). GDF15, a secreted protein, has been implicated in promoting retinal ganglion-cell differentiation in the developing retina in rodent retinal progenitor cells and human embryonic stem cells.[62] MDK, a heparin-binding growth factor, plays a significant role in the maintenance of pluripotency in stem cells[63] and the regulation of lineage commitment in various developmental contexts.[64] It serves as a regulator in the neural specification and promotes survival of differentiating cells. GPNMB, a transmembrane glycoprotein, has been shown to facilitate the differentiation of neural progenitor cells into mature neurons[65,66] and to promote the odontoblastic differentiation of human dental pulp cells.[67] Collectively, these genes in Cluster 3 likely contribute to the regulation of stem cell differentiation processes, particularly in the context of spheroid formation and neural differentiation (Fig. 4B). The higher responses of these upregulated genes to the H3K9me3 inhibitor further suggested the importance of H3K9me3 in regulating the signaling network for neural lineage differentiation in Cluster 3 cells during spheroid formation (Table 1).

The high expression of APOE, DUSP1, NUPR1, NEUROG1, and SOX4 genes in both Clusters 3 and 6 suggests that chitosan-induced spheroids are also involved in various processes related to neuronal differentiation, maturation, and function (Fig. 3C). APOE, a multifunctional protein involved in lipid metabolism and transport, plays a critical role in neuronal development, synaptic plasticity, and repair following injury.[68] In the adult central nervous system, APOE is mainly expressed by astrocytes and acts as a negative regulator of cell proliferation. However, during development, APOE expression by neural stem cells promotes neurosphere formation and gliogenesis.[69,70] DUSP1 plays a crucial role in regulating signaling pathways essential for neurogenesis, neuronal differentiation, and apoptosis.[71] NUPR1, an upstream regulator of p53, is implicated in neurogenesis and neuronal differentiation.[72,73] NEUROG1 is a transcription factor that promotes neuronal fate determination.[74] Furthermore, SOX4 is a transcription factor known for its important roles in regulating neural stem cell maintenance, neuronal differentiation, and gliogenesis.[75] It controls gene expression that directs the fate determination of neural stem cells, promoting their self-renewal and preventing premature differentiation.[76] The combined percentage of Clusters 6 and 3 cells accounts for approximately 40% of the spheroid population. The inductions of the aforementioned genes indicate the inclination of ASCs toward neuronal lineage following exposure to a chitosan-coated surface (Fig. 4C).

ASCs spheroid formation is a spontaneous cell assembly process that occurs after seeding cells on the chitosan-coated surface in the current study. Self-assembly happens during embryogenesis, morphogenesis, and organogenesis that can be modulated by chemical, cellular, and microenvironmental factors.[77] Various methods have been developed to promote sphere formation of MSCs, including the hanging drop, gel embedding, magnetic levitation, and spinner culture. Spheroid culture of ASCs or MSCs promotes the expression of stemness marker such as Oct4 and Nanog transcription factors and secretory factors important for cell viability, migration, and tissue regenerations.[78,79] Cadherin and integrin-related signaling networks play important roles in the formation of multicellular spheroids by aggregating single suspending cells to form loosely adhesive cells and then creating homophilic binding through E-cadherin and β-catenin complex to form strong adhesion in spheroid.[80,81] The multicellular systems in 3D, such as organoids, assembloids, and/or organ-on-chip models, have been viciously developed to mimic the organ function for studying cancer, genetic disorders, infectious diseases, and neurological diseases.[82,83] Brain region-specific organoids and/or spheroids have been established to study the functional cell–cell interactions for artificial fetal forebrain,[84] neural circuits,[85] and cortico-motor interactions.[86] Transplantation of MSC spheroids induced by BDNF transfection promotes motor recovery in mice with thoracic spinal cord injury.[87] Although recent developments in scRNA-seq and other spatial imaging transcriptomics approaches have allowed for the study of cell heterogeneity and the identification of specific cell populations using tools like CellPhoneDB, NicheNet, iTalk, CellTalker, and CellChat,[82] the detailed understanding of cell-cell interactions and cell-microenvironmental interactions in spheroids and organoids, particularly regarding the epigenetic regulation, still needs further investigation. This study provides insights into the epigenetic regulatory mechanisms during spheroid formation and can be used to promote the development of neurospheroids for nerve repair. Furthermore, the identified gene responsible for driving stem cell differentiation into the neural lineage, as well as the isolation of subpopulations within clusters 6 and cluster 3, hold promise as potential therapeutic strategies to target specific gene expression and regulatory pathways to enhance neural repair and regeneration.

Conclusion

Histone trimethylation at H3K4, H3K9, and H3K27 was robustly induced during the formation of spheroids by ASCs, accompanied by an increase in histone deacetylase expression and a marked reduction in histone acetylation. The translocation of HDAC5 from the cytoplasm to the nucleus further confirms its involvement in this process. Through single-cell RNA sequencing and rigorous cell fate trajectory analyses, we have identified distinct cell populations within the spheroids. Notably, Cluster 3 cells represent the endpoint state, while Cluster 6 cells tentatively signify a transient subpopulation during chitosan-induced spheroid formation. Inhibition experiments using specific inhibitors further validated the significance of histone trimethylation and HDAC5 in neural spheroid formation and revealed specific genes involved in stem cell differentiation and lineage commitment. Our findings discovered the dominant role of H3K4me3 in governing the transient state, as exemplified by Cluster 6 cells, while H3K9me3 and HDAC5 preside over the endpoint stage observed in Cluster

3 cells. Taken together, these findings underscore the crucial role of epigenetic regulation, particularly H3K4me3 and H3K9me3, in shaping cell fate and directing lineage-specific differentiation.

Acknowledgments

We are grateful for the optical microscopy technical services provided by Bioimaging Core Facility of the National Core Facility for Biopharmaceuticals, National Science and Technology Council, Taiwan, and the Core Research Laboratory, College of Medicine, National Cheng Kung University, Taiwan. We also thank the National Core Facility for Biopharmaceuticals (NCFB111-2740-B-492-001) and the National Center for High-performance Computing (NCHC) of National Applied Research Laboratories (NARLabs) of Taiwan for providing computational resources and storage resources.

Funding

This study was financially supported by grants from National Science and Technology Council, Taiwan [NSTC111-2320-B-006-069-MY2(MMC), MOST111-2311-B-006-003(CCW), MOST110-2320-B006-029-MY3(CCW), and MOST110-2311-B-006-007(CCW)] and the National Health Research Institutes of Taiwan (NHRI-EX111-10925EI; CCW). The funding body played no role in the design of the study and collection, analysis, and interpretation of data and in writing the manuscript.

Conflict of Interest

The authors indicated no financial relationships.

Author Contributions

M.M.C.: conception and design of the study, perform all experiments, data collection and analysis, financial support, manuscript writing, final approval of the manuscript. Y.K.H.: perform scRNA-seq experiments, collection of scRNA-seq data, data analysis and interpretation, final approval of the manuscript. C.K.H.: interpreted and provided important strategic analysis of scRNA-seq results, provision of study material, final approval of the manuscript. H.I.C.H.: interpreted and provided important strategic analysis of scRNA-seq results, final approval of the manuscript. B.M.H.: provision of study material, final approval of the manuscript. Y.H.L.: discussion of the study, data analysis, final approval of the manuscript. F.I.L., S.P.L.: discussion of the study, data analysis and provide experimental support, final approval of the manuscript. Y.Y.H.: discussion of the study, provision of study material, final approval of the manuscript. C.C.W: conception and design the study, administrative support, data collection and analysis, financial support, manuscript writing, final approval of the manuscript.

Data Availability

All data generated and analyzed during this study are included in this published article and its supplementary materials. Additional experimental details and more detailed data used or analyzed during the current study are available from the corresponding author upon reasonable request. The scRNA-seq data reported in this article have been deposited in NCBI's Gene Expression Omnibus (GEO) and are accessible through GEO Series accession number.

Supplementary Material

Supplementary material is available at *Stem Cells Translational Medicine* online.

References

1. Pittenger MF, Discher DE, Peault BM, et al. Mesenchymal stem cell perspective: cell biology to clinical progress. *NPJ Regen Med*. 2019;4:22. https://doi.org/10.1038/s41536-019-0083-6
2. Zuk PA. The adipose-derived stem cell: looking back and looking ahead. *Mol Biol Cell*. 2010;21(11):1783–1787. https://doi.org/10.1091/mbc.e09-07-0589
3. Graf T. Historical origins of transdifferentiation and reprogramming. *Cell Stem Cell*. 2011;9(6):504–516. https://doi.org/10.1016/j.stem.2011.11.012
4. Mascharak S, Talbott HE, Januszyk M, et al. Multi-omic analysis reveals divergent molecular events in scarring and regenerative wound healing. *Cell Stem Cell*. 2022;29(2):315–327.e6. https://doi.org/10.1016/j.stem.2021.12.011
5. Wang YH, Guo YC, Wang DR, Liu JY, Pan J. Adipose stem cell-based clinical strategy for neural regeneration: a review of current opinion. *Stem Cells Int*. 2019;2019:8502370. https://doi.org/10.1155/2019/8502370
6. Piovesana R, Faroni A, Tata AM, Adam J, Reid AJ. Schwann-like adipose-derived stem cells as a promising therapeutic tool for peripheral nerve regeneration: effects of cholinergic stimulation. *Neural Regener Res*. 2021;16(6):1218–1220. https://doi.org/10.4103/1673-5374.300433
7. Mohamed-Ahmed S, Fristad I, Lie SA, et al. Adipose-derived and bone marrow mesenchymal stem cells: a donor-matched comparison. *Stem Cell Res Ther*. 2018;9(1):168. https://doi.org/10.1186/s13287-018-0914-1
8. He Y, Lin S, Ao Q, He X. The co-culture of ASCs and EPCs promotes vascularized bone regeneration in critical-sized bone defects of cranial bone in rats. *Stem Cell Res Ther*. 2020;11(1):338. https://doi.org/10.1186/s13287-020-01858-6
9. Mohamed-Ahmed S, Yassin MA, Rashad A, et al. Comparison of bone regenerative capacity of donor-matched human adipose-derived and bone marrow mesenchymal stem cells. *Cell Tissue Res*. 2021;383(3):1061–1075. https://doi.org/10.1007/s00441-020-03315-5
10. Hiwatashi N, Hirano S, Mizuta M, et al. Adipose-derived stem cells versus bone marrow-derived stem cells for vocal fold regeneration. *Laryngoscope*. 2014;124(12):E461–E469. https://doi.org/10.1002/lary.24816
11. Ma T, Sun J, Zhao Z, et al. A brief review: adipose-derived stem cells and their therapeutic potential in cardiovascular diseases. *Stem Cell Res Ther*. 2017;8(1):124. https://doi.org/10.1186/s13287-017-0585-3
12. Santos AK, Gomes KN, Parreira RC, et al. Mouse neural stem cell differentiation and human adipose mesenchymal stem cell transdifferentiation into neuron- and oligodendrocyte-like cells with myelination potential. *Stem Cell Rev Rep*. 2022;18(2):732–751. https://doi.org/10.1007/s12015-021-10218-7
13. Radhakrishnan S, Trentz OA, Reddy MS, et al. In vitro transdifferentiation of human adipose tissue-derived stem cells to neural lineage cells—a stage-specific incidence. *Adipocyte*. 2019;8(1):164–177. https://doi.org/10.1080/21623945.2019.1607424
14. Si Z, Wang X, Sun C, et al. Adipose-derived stem cells: sources, potency, and implications for regenerative therapies. *Biomed Pharmacother*. 2019;114:108765. https://doi.org/10.1016/j.biopha.2019.108765
15. Kang SK, Putnam LA, Ylostalo J, et al. Neurogenesis of Rhesus adipose stromal cells. *J Cell Sci*. 2004;117(Pt 18):4289–4299. https://doi.org/10.1242/jcs.01264

16. Salehi H, Amirpour N, Niapour A, Razavi S. An overview of neural differentiation potential of human adipose derived stem cells. *Stem Cell Rev Rep*. 2016;12(1):26–41. https://doi.org/10.1007/s12015-015-9631-7
17. Huang CW, Lu SY, Huang TC, et al. FGF9 induces functional differentiation to Schwann cells from human adipose derived stem cells. *Theranostics*. 2020;10(6):2817–2831. https://doi.org/10.7150/thno.38553
18. Cardozo AJ, Gomez DE, Argibay PF. Neurogenic differentiation of human adipose-derived stem cells: relevance of different signaling molecules. *Gene*. 2012;511(2):427–436. https://doi.org/10.1016/j.gene.2012.09.038
19. Cai S, Tsui YP, Tam KW, et al. Directed differentiation of human bone marrow stromal cells to fate-committed Schwann cells. *Stem Cell Rep*. 2017;9(4):1097–1108. https://doi.org/10.1016/j.stemcr.2017.08.004
20. Tsui YP, Lam G, Wu KL, et al. Derivation of oligodendrocyte precursors from adult bone marrow stromal cells for remyelination therapy. *Cells*. 2021;10(8):2166. https://doi.org/10.3390/cells10082166
21. Shea GK, Tai EW, Leung KH, et al. Juxtacrine signalling via Notch and ErbB receptors in the switch to fate commitment of bone marrow-derived Schwann cells. *Eur J Neurosci*. 2020;52(5):3306–3321. https://doi.org/10.1111/ejn.14837
22. Sun X, Zhu Y, Yin HY, et al. Differentiation of adipose-derived stem cells into Schwann cell-like cells through intermittent induction: potential advantage of cellular transient memory function. *Stem Cell Res Ther*. 2018;9(1):133. https://doi.org/10.1186/s13287-018-0884-3
23. Hsueh YY, Chang YJ, Huang TC, et al. Functional recoveries of sciatic nerve regeneration by combining chitosan-coated conduit and neurosphere cells induced from adipose-derived stem cells. *Biomaterials*. 2014;35(7):2234–2244. https://doi.org/10.1016/j.biomaterials.2013.11.081
24. Hsueh YY, Chiang YL, Wu CC, Lin SC. Spheroid formation and neural induction in human adipose-derived stem cells on a chitosan-coated surface [Research Support, Non-U.S. Gov't]. *Cells Tissues Organs*. 2012;196(2):117–128. https://doi.org/10.1159/000332045
25. Cheng NC, Wang S, Young TH. The influence of spheroid formation of human adipose-derived stem cells on chitosan films on stemness and differentiation capabilities. *Biomaterials*. 2012;33(6):1748–1758. https://doi.org/10.1016/j.biomaterials.2011.11.049
26. Volker-Albert M, Bronkhorst A, Holdenrieder S, Imhof A. Histone modifications in stem cell development and their clinical implications. *Stem Cell Rep*. 2020;15(6):1196–1205. https://doi.org/10.1016/j.stemcr.2020.11.002
27. Swygert SG, Peterson CL. Chromatin dynamics: interplay between remodeling enzymes and histone modifications. *Biochim Biophys Acta*. 2014;1839(8):728–736. https://doi.org/10.1016/j.bbagrm.2014.02.013
28. Bhanu NV, Sidoli S, Garcia BA. Histone modification profiling reveals differential signatures associated with human embryonic stem cell self-renewal and differentiation. *Proteomics*. 2016;16(3):448–458. https://doi.org/10.1002/pmic.201500231
29. Bernstein BE, Mikkelsen TS, Xie X, et al. A bivalent chromatin structure marks key developmental genes in embryonic stem cells. *Cell*. 2006;125(2):315–326. https://doi.org/10.1016/j.cell.2006.02.041
30. Harikumar A, Meshorer E. Chromatin remodeling and bivalent histone modifications in embryonic stem cells. *EMBO Rep*. 2015;16(12):1609–1619. https://doi.org/10.15252/embr.201541011
31. Voigt P, Tee WW, Reinberg D. A double take on bivalent promoters. *Genes Dev*. 2013;27(12):1318–1338. https://doi.org/10.1101/gad.219626.113
32. Boulland JL, Mastrangelopoulou M, Boquest AC, et al. Epigenetic regulation of nestin expression during neurogenic differentiation of adipose tissue stem cells. *Stem Cells Dev*. 2013;22(7):1042–1052. https://doi.org/10.1089/scd.2012.0560
33. Trisciuoglio D, Di Martile M, Del Bufalo D. Emerging role of histone acetyltransferase in stem cells and cancer. *Stem Cells Int*. 2018;2018:8908751. https://doi.org/10.1155/2018/8908751
34. Mu X, Yan S, Fu C, Wei A. The histone acetyltransferase MOF promotes induces generation of pluripotent stem cells. *Cell Reprogram*. 2015;17(4):259–267. https://doi.org/10.1089/cell.2014.0102
35. Zhang P, Liu Y, Jin C, et al. Histone acetyltransferase GCN5 regulates osteogenic differentiation of mesenchymal stem cells by inhibiting NF-kappaB. *J Bone Miner Res*. 2016;31(2):391–402. https://doi.org/10.1002/jbmr.2704
36. He R, Dantas A, Riabowol K. Histone acetyltransferases and stem cell identity. *Cancers (Basel)*. 2021;13(10):2407. https://doi.org/10.3390/cancers13102407
37. Khokhar ES, Borikar S, Eudy E, et al. Aging-associated decrease in the histone acetyltransferase KAT6B is linked to altered hematopoietic stem cell differentiation. *Exp Hematol*. 2020;82:43–52.e4. https://doi.org/10.1016/j.exphem.2020.01.014
38. Acharya D, Hainer SJ, Yoon Y, et al. KAT-independent gene regulation by Tip60 promotes ESC self-renewal but not pluripotency. *Cell Rep*. 2017;19(4):671–679. https://doi.org/10.1016/j.celrep.2017.04.001
39. Jamaladdin S, Kelly RD, O'Regan L, et al. Histone deacetylase (HDAC) 1 and 2 are essential for accurate cell division and the pluripotency of embryonic stem cells. *Proc Natl Acad Sci USA*. 2014;111(27):9840–9845. https://doi.org/10.1073/pnas.1321330111
40. Nieto-Estevez V, Changarathil G, Adeyeye AO, et al. HDAC1 regulates neuronal differentiation. *Front Mol Neurosci*. 2021;14:815808. https://doi.org/10.3389/fnmol.2021.815808
41. Pon JR, Marra MA. MEF2 transcription factors: developmental regulators and emerging cancer genes. *Oncotarget*. 2016;7(3):2297–2312. https://doi.org/10.18632/oncotarget.6223
42. Cho Y, Cavalli V. HDAC5 is a novel injury-regulated tubulin deacetylase controlling axon regeneration. *EMBO J*. 2012;31(14):3063–3078. https://doi.org/10.1038/emboj.2012.160
43. Cockburn K, Annusver K, Gonzalez DG, et al. Gradual differentiation uncoupled from cell cycle exit generates heterogeneity in the epidermal stem cell layer. *Nat Cell Biol*. 2022;24(12):1692–1700. https://doi.org/10.1038/s41556-022-01021-8
44. Sainz de la Maza D, Hof-Michel S, Phillimore L, Bokel C, Amoyel M. Cell-cycle exit and stem cell differentiation are coupled through regulation of mitochondrial activity in the *Drosophila testis*. *Cell Rep*. 2022;39(6):110774. https://doi.org/10.1016/j.celrep.2022.110774
45. Kompisch KM, Lange C, Steinemann D, et al. Neurogenic transdifferentiation of human adipose-derived stem cells? A critical protocol reevaluation with special emphasis on cell proliferation and cell cycle alterations. *Histochem Cell Biol*. 2010;134(5):453–468. https://doi.org/10.1007/s00418-010-0740-8
46. Bloom J, Cross FR. Multiple levels of cyclin specificity in cell-cycle control. *Nat Rev Mol Cell Biol*. 2007;8(2):149–160. https://doi.org/10.1038/nrm2105
47. Frontini M, Kukalev A, Leo E, et al. The CDK subunit CKS2 counteracts CKS1 to control cyclin A/CDK2 activity in maintaining replicative fidelity and neurodevelopment. *Dev Cell*. 2012;23(2):356–370. https://doi.org/10.1016/j.devcel.2012.06.018
48. Liu L, Michowski W, Kolodziejczyk A, Sicinski P. The cell cycle in stem cell proliferation, pluripotency and differentiation. *Nat Cell Biol*. 2019;21(9):1060–1067. https://doi.org/10.1038/s41556-019-0384-4
49. Hsueh YY, Chang YJ, Huang CW, et al. Synergy of endothelial and neural progenitor cells from adipose-derived stem cells to preserve neurovascular structures in rat hypoxic-ischemic brain injury. *Sci Rep*. 2015;5:14985. https://doi.org/10.1038/srep14985
50. Qiu X, Mao Q, Tang Y, et al. Reversed graph embedding resolves complex single-cell trajectories. *Nat Methods*. 2017;14(10):979–982. https://doi.org/10.1038/nmeth.4402
51. Zhang H, Chen Y, Fan C, et al. Cell-subpopulation alteration and FGF7 activation regulate the function of tendon stem/progenitor cells in 3D microenvironment revealed by single-cell analysis. *Biomaterials*. 2022;280:121238. https://doi.org/10.1016/j.biomaterials.2021.121238

52. Huang Y, Hamana T, Liu J, et al. Type 2 fibroblast growth factor receptor signaling preserves stemness and prevents differentiation of prostate stem cells from the basal compartment. *J Biol Chem*. 2015;290(29):17753–17761. https://doi.org/10.1074/jbc.M115.661066
53. Reza AM, Lee S, Shiwani S, Singh NK. KGF and BMP-6 intervene in cellular reprogramming and in mesenchymal-epithelial transition (MET) of 3T3L1 mouse adipose cells. *Cell Biol Int*. 2015;39(4):400–410. https://doi.org/10.1002/cbin.10407
54. Goessling W, North TE, Loewer S, et al. Genetic interaction of PGE2 and Wnt signaling regulates developmental specification of stem cells and regeneration. *Cell*. 2009;136(6):1136–1147. https://doi.org/10.1016/j.cell.2009.01.015
55. Niringiyumukiza JD, Cai H, Xiang W. Prostaglandin E2 involvement in mammalian female fertility: ovulation, fertilization, embryo development and early implantation. *Reprod Biol Endocrinol*. 2018;16(1):43. https://doi.org/10.1186/s12958-018-0359-5
56. Gudas LJ, Wagner JA. Retinoids regulate stem cell differentiation. *J Cell Physiol*. 2011;226(2):322–330. https://doi.org/10.1002/jcp.22417
57. Semrau S, Goldmann JE, Soumillon M, et al. Dynamics of lineage commitment revealed by single-cell transcriptomics of differentiating embryonic stem cells. *Nat Commun*. 2017;8(1):1096. https://doi.org/10.1038/s41467-017-01076-4
58. De Angelis MT, Parrotta EI, Santamaria G, Cuda G. Short-term retinoic acid treatment sustains pluripotency and suppresses differentiation of human induced pluripotent stem cells. *Cell Death Dis*. 2018;9(1):6. https://doi.org/10.1038/s41419-017-0028-1
59. Patel J, Xun D, Creswell K, et al. Loss of RARRES1 function promotes follicular lymphomagenesis and inhibits B cell differentiation in mice. *Int J Biol Sci*. 2022;18(7):2670–2682. https://doi.org/10.7150/ijbs.69615
60. Llorens-Bobadilla E, Zhao S, Baser A, et al. Single-cell transcriptomics reveals a population of dormant neural stem cells that become activated upon brain injury. *Cell Stem Cell*. 2015;17(3):329–340. https://doi.org/10.1016/j.stem.2015.07.002
61. Pellegrini S, Chimienti R, Scotti GM, et al. Transcriptional dynamics of induced pluripotent stem cell differentiation into beta cells reveals full endodermal commitment and homology with human islets. *Cytotherapy*. 2021;23(4):311–319. https://doi.org/10.1016/j.jcyt.2020.10.004
62. Chang KC, Sun C, Cameron EG, et al. Opposing effects of growth and differentiation factors in cell-fate specification. *Curr Biol*. 2019;29(12):1963–1975.e5. https://doi.org/10.1016/j.cub.2019.05.011
63. Zhao SL, Zhang YJ, Li MH, Zhang XL, Chen SL. Mesenchymal stem cells with overexpression of midkine enhance cell survival and attenuate cardiac dysfunction in a rat model of myocardial infarction. *Stem Cell Res Ther*. 2014;5(2):37. https://doi.org/10.1186/scrt425
64. Singec I, Crain AM, Hou J, et al. Quantitative analysis of human pluripotency and neural specification by in-depth (phospho)proteomic profiling. *Stem Cell Rep*. 2016;7(3):527–542. https://doi.org/10.1016/j.stemcr.2016.07.019
65. Magri L, Cambiaghi M, Cominelli M, et al. Sustained activation of mTOR pathway in embryonic neural stem cells leads to development of tuberous sclerosis complex-associated lesions. *Cell Stem Cell*. 2011;9(5):447–462. https://doi.org/10.1016/j.stem.2011.09.008
66. Kawahara K, Hirata H, Ohbuchi K, et al. The novel monoclonal antibody 9F5 reveals expression of a fragment of GPNMB/osteoactivin processed by furin-like protease(s) in a subpopulation of microglia in neonatal rat brain. *Glia*. 2016;64(11):1938–1961. https://doi.org/10.1002/glia.23034
67. Wang YL, Hu YJ, Zhang FH. Effects of GPNMB on proliferation and odontoblastic differentiation of human dental pulp cells. *Int J Clin Exp Pathol*. 2015;8(6):6498–6504.
68. Gan HT, Tham M, Hariharan S, et al. Identification of ApoE as an autocrine/paracrine factor that stimulates neural stem cell survival via MAPK/ERK signaling pathway. *J Neurochem*. 2011;117(3):565–578. https://doi.org/10.1111/j.1471-4159.2011.07227.x
69. Dause TJ, Denninger JK, Smith BM, Kirby ED. The neural stem cell secretome across neurodevelopment. *Exp Neurol*. 2022;355:114142. https://doi.org/10.1016/j.expneurol.2022.114142
70. Tensaouti Y, Stephanz EP, Yu TS, Kernie SG. ApoE regulates the development of adult newborn hippocampal neurons. *eNeuro*. 2018;5(4):e0155-18.2018 1-15. https://doi.org/10.1523/ENEURO.0155-18.2018
71. An N, Bassil K, Al Jowf GI, et al. Dual-specificity phosphatases in mental and neurological disorders. *Prog Neurobiol*. 2021;198:101906. https://doi.org/10.1016/j.pneurobio.2020.101906
72. Tsampoula M, Tarampoulous I, Manolakou T, Ninou E, Politis PK. The neurodevelopmental disorders associated gene Rnf113a regulates survival and differentiation properties of neural stem cells. *Stem Cells*. 2022;40(7):678–690. https://doi.org/10.1093/stmcls/sxac030
73. Hidaka R, Machida M, Fujimaki S, et al. Monitoring neurodegeneration in diabetes using adult neural stem cells derived from the olfactory bulb. *Stem Cell Res Ther*. 2013;4(3):51. https://doi.org/10.1186/scrt201
74. Dixit R, Wilkinson G, Cancino GI, et al. Neurog1 and Neurog2 control two waves of neuronal differentiation in the piriform cortex. *J Neurosci*. 2014;34(2):539–553. https://doi.org/10.1523/JNEUROSCI.0614-13.2014
75. Braccioli L, Vervoort SJ, Puma G, Nijboer CH, Coffer PJ. SOX4 inhibits oligodendrocyte differentiation of embryonic neural stem cells in vitro by inducing Hes5 expression. *Stem Cell Res*. 2018;33:110–119. https://doi.org/10.1016/j.scr.2018.10.005
76. Bhattaram P, Penzo-Mendez A, Sock E, et al. Organogenesis relies on SoxC transcription factors for the survival of neural and mesenchymal progenitors. *Nat Commun*. 2010;1(1):9. https://doi.org/10.1038/ncomms1008
77. Ryu NE, Lee SH, Park H. Spheroid culture system methods and applications for mesenchymal stem cells. *Cells*. 2019;8(12):1620. https://doi.org/10.3390/cells8121620
78. Cheng NC, Chen SY, Li JR, Young TH. Short-term spheroid formation enhances the regenerative capacity of adipose-derived stem cells by promoting stemness, angiogenesis, and chemotaxis. *Stem Cells Transl Med*. 2013;2(8):584–594. https://doi.org/10.5966/sctm.2013-0007
79. Ho SS, Murphy KC, Binder BY, Vissers CB, Leach JK. Increased survival and function of mesenchymal stem cell spheroids entrapped in instructive alginate hydrogels. *Stem Cells Transl Med*. 2016;5(6):773–781. https://doi.org/10.5966/sctm.2015-0211
80. Tsai AC, Liu Y, Yuan X, Ma T. Compaction, fusion, and functional activation of three-dimensional human mesenchymal stem cell aggregate. *Tissue Eng Part A*. 2015;21(9–10):1705–1719. https://doi.org/10.1089/ten.TEA.2014.0314
81. Konze SA, van Diepen L, Schroder A, et al. Cleavage of E-cadherin and beta-catenin by calpain affects Wnt signaling and spheroid formation in suspension cultures of human pluripotent stem cells. *Mol Cell Proteomics*. 2014;13(4):990–1007. https://doi.org/10.1074/mcp.M113.033423
82. Goldrick C, Guri I, Herrera-Oropeza G, et al. 3D multicellular systems in disease modelling: from organoids to organ-on-chip. *Front Cell Dev Biol*. 2023;11:1083175. https://doi.org/10.3389/fcell.2023.1083175
83. Vogt N. Assembloids. *Nat Methods*. 2021;18(1):27. https://doi.org/10.1038/s41592-020-01026-x
84. Birey F, Andersen J, Makinson CD, et al. Assembly of functionally integrated human forebrain spheroids. *Nature*. 2017;545(7652):54–59. https://doi.org/10.1038/nature22330
85. Miura Y, Li MY, Revah O, et al. Engineering brain assembloids to interrogate human neural circuits. *Nat Protoc*. 2022;17(1):15–35. https://doi.org/10.1038/s41596-021-00632-z
86. Panoutsopoulos AA. Organoids, assembloids, and novel biotechnology: steps forward in developmental and disease-related neuroscience. *Neuroscientist*. 2021;27(5):463–472. https://doi.org/10.1177/1073858420960112
87. Uchida S, Hayakawa K, Ogata T, et al. Treatment of spinal cord injury by an advanced cell transplantation technology using brain-derived neurotrophic factor-transfected mesenchymal stem cell spheroids. *Biomaterials*. 2016;109:1–11. https://doi.org/10.1016/j.biomaterials.2016.09.007